

De Novo Computational Prediction of Non-coding RNA Genes in Prokaryotic Genomes

Thao T. Tran^{1,2,*}, Fengfeng Zhou², Sarah Marshburn³, Mark Stead³, Sidney R. Kushner³ and Ying Xu^{2,4}

¹School of Electrical and Computer Engineering, Georgia Institute of Technology, Atlanta, GA, USA

²Computational Systems Biology Laboratory, Department of Biochemistry and Molecular Biology, Institute of Bioinformatics and BioEnergy Science Center (BESC), University of Georgia, Athens, GA, USA

³Department of Genetics, University of Georgia, Athens, GA, USA

⁴College of Computer Science and Technology, Jilin University, Changchun, China

Associate Editor: Prof. Ivo Hofacker

ABSTRACT

Motivation: The computational identification of non-coding RNA (ncRNA) genes represents one of the most important and challenging problems in computational biology. Existing methods for ncRNA gene prediction rely mostly on homology information, thus limiting their applications to ncRNA genes with known homologues.

Results: We present a novel *de novo* prediction algorithm for ncRNA genes using features derived from the sequences and structures of known ncRNA genes in comparison to decoys. Using these features, we have trained a neural network-based classifier and have applied it to *E. coli* and *S. solfataricus* for genome-wide prediction of ncRNAs. Our method has an average prediction sensitivity and specificity of 68% and 70%, respectively, for identifying windows with potential for ncRNA genes in *E. coli*. By combining windows of different sizes and using positional filtering strategies, we predicted 601 candidate ncRNAs and recovered 41% of known ncRNAs in *E. coli*. We experimentally investigated six novel candidates using Northern blot analysis and found expression of three candidates: one represents a potential new ncRNA, one is associated with stable mRNA decay intermediates, and one is a case of either a potential riboswitch or transcription attenuator involved in the regulation of cell division. In general, our approach enables the identification of both *cis*- and *trans*- acting ncRNAs in partially or completely sequenced microbial genomes without requiring homology or structural conservation.

Availability: The source code and results are available at <http://csbl.bmb.uga.edu/publications/materials/tran/>.

1 INTRODUCTION

Non-coding RNA (ncRNA) or small RNA (sRNA) genes, which encode functional RNA molecules that are not translated into proteins, are involved in a variety of cellular processes ranging from regulation of gene expression to RNA modification and editing (Gottesman, 2005; Huttenhofer, et al., 2002). In humans, it is estimated that about 98% of the genome can be transcribed, of which only ~2% encodes protein genes (Szymanski, et al., 2003), suggesting the possibility that a large percentage of the genome may encode ncRNA genes. Although the vital importance of ncRNA genes in cellular activities is well recognized, our current knowledge about the collection of all ncRNA genes encoded in a particular genome is very limited because of the lack of effective capabilities, either computational or experimental, for elucidating them.

It is generally believed that the identification of ncRNA genes, particularly in bacterial genomes, is more challenging than protein-coding genes. Unlike protein-coding genes, ncRNA genes do not contain easily detectable signals such as open reading frames (i.e., a sequence between an in-frame start codon and the first in-frame stop codon going from the 5' to the 3' end of the sequence), codon biases, or ribosome binding sites. Although some ncRNA genes have recognizable promoters and terminators (Argaman, et al., 2001; Chen, et al., 2002), the identification of such regulatory signals is quite challenging. This identification problem is further complicated by the fact that most ncRNA genes are much shorter than protein-coding genes.

A number of computational methods for identifying ncRNA genes have been developed and reported (Argaman, et al., 2001; Chen, et al., 2002; Klein, et al., 2002; Livny, et al., 2005; Pichon and Felden, 2003; Schattner, 2002; Washietl, et al., 2005; Wassarman, et al., 2001; Yachie, et al., 2006; Zhang, et al., 2004). These methods generally fall into two classes: (1) methods that identify members of an ncRNA family based on homology information (Argaman, et al., 2001; Wassarman, et al., 2001) and (2) methods that find novel ncRNAs based on general features common to ncRNA genes. We focus on the latter class of methods since it relates to our approach.

Two classes of methods have been developed to predict novel ncRNAs. The first one identifies conserved and relatively long sequences in the intergenic regions across closely related genomes. This type of method is based on the assumption, which is generally true for prokaryotic genomes, that such conserved regions encode functional RNAs and not *cis*-regulatory DNA motifs. Such a strategy has been used to mine *E. coli* (Zhang, et al., 2004) and other bacterial genomes (Pichon and Felden, 2003) for novel ncRNAs. By limiting the search to intergenic regions, one could realistically search for ncRNA genes on a genome-wide scale. However, this approach will miss ncRNAs that overlap protein-coding genes, either sense or antisense, and ncRNA genes that are unique to a genome. For example, it is known that ~25% of the *C/D* snoRNA genes overlap protein-coding genes in the *Pyrococcus abyssi* genome (Gaspin, et al., 2000). A generalization of this type of method is to predict novel ncRNA genes through the identification of conserved RNA secondary structures across related genomes and further analyze their mutational patterns (Rivas and Eddy, 2001; Rivas, et al., 2001) or evaluate the folding energy of their

*To whom correspondence should be addressed.

predicted structures (Coventry, et al., 2004; di Bernardo, et al., 2003; Pedersen, et al., 2006; Washietl, et al., 2005). These structure-based methods rely on the need for homology alignments as well as having high quality alignments .

The second class of approach predicts novel ncRNA genes based on identifying both common and distinguishing features of known ncRNA genes in target genomic regions. The features used have included predicted promoters and terminators, as well as the base compositions of target sequences. Typical requirements mandate that such a region be short and flanked by promoter and terminator signals (Argaman, et al., 2001; Chen, et al., 2002). Clearly, such methods are limited in their effectiveness in reliable prediction of novel ncRNA genes for two main reasons: (a) accurate prediction of such signals is very challenging and unreliable, and (b) only a fraction of terminators, namely, rho-independent terminators in prokaryotes, can be computationally predicted (Kingsford, et al., 2007).

Although nucleotide composition-based methods have had some success in ncRNA gene prediction, these methods are limited to organisms with compositional bias in their ncRNA genes in relation to their underlying genome. For example, in A/T-rich hyperthermophilic genomes, the ncRNA genes are relatively more GC-rich (Klein, et al., 2002; Larsson, et al., 2008; Schattner, 2002). In addition to base composition (or mono-nucleotide composition), some programs have employed di- and tri-nucleotide frequencies to distinguish ncRNA genes from the genomic background (Wang, et al., 2006). Such information has also been further enhanced through the use of folding energy and known RNA motifs (Carter, et al., 2001) for the prediction of ncRNA genes in *E. coli*.

In this paper, we present a *de novo* method for predicting ncRNAs in bacterial genomes that employs a number of novel structural features associated with known ncRNA genes. Our method does not require prior homology, multiple sequence alignments, or structural conservation but uses only sequence and structure-based features easily derivable from the genome itself, which is a major advantage since the method can be directly applied to any organism that may be newly sequenced or partially sequenced. A neural network-based classifier was trained to predict the ncRNA genes on a genome-wide scale. We have applied this classifier to RNA gene prediction in *E. coli* and have compared our predictions to other existing programs. Furthermore, we also experimentally investigated six of the novel candidate ncRNAs predicted by the algorithm using Northern blot analysis, and identified a potential new ncRNA located downstream of the *ydgA* gene as well as a *cis*-acting regulatory element that helps control the expression of the essential *mreB* operon.

2 METHODS

To train a classifier for the *de novo* prediction of ncRNAs genes, we first generated a positive data set containing known ncRNA genes and identified a set of sequence and structural-based features that could distinguish the positive data set from non-ncRNA genes. We assumed that ncRNA genes are no longer than 1,000 nucleotides (nt), which covers the vast majority of the known ncRNAs in prokaryotes. We refer the reader to the Supplementary Materials for additional details presented in each of the following subsections.

2.1 Data set generation

Our positive ncRNA data set was derived from three existing sources: (1) the NONCODE database (Liu, et al., 2005), (2) published literature, and (3) GenBank. These searches yielded 427, 426, and 1,105 ncRNAs from NONCODE, published literature, and NCBI, respec-

tively, for a total of 1,540 non-overlapping ncRNAs, which we refer to as “*Positive1540*” for future reference.

To remove redundant sequences from within this data set, we applied the Markov cluster (MCL) algorithm to group together similar sequences using the default inflation parameter and a BLAST bit-score cutoff of 5 (Enright, et al., 2002). Our application of this algorithm resulted in 936 clusters from which we randomly selected one ncRNA from each cluster to use in our final training data set. We refer to this data set as “*Positive936*” to represent our positive controls.

The generation of the negative control represented a challenge in our work since there are no known negative sets, i.e., regions of the genome known not to contain ncRNA genes. Approaches using segments of the genomic background (Carter, et al., 2001; Saetrom, et al., 2005; Schattner, 2002) as the control inherently assume that ncRNA genes make up only a small portion of the entire genome, which may not be correct. Other methods use randomly shuffled permutations of known ncRNA genes to build a negative training data set (Clote, et al., 2005; Klein, et al., 2002; Rivas and Eddy, 2000; Workman and Krogh, 1999). We constructed our negative set by shuffling sequences of known ncRNA genes, while preserving both the mono- and di-nucleotide frequencies. This approach prevented the negative set from being biased to certain regions of the genome. The rationale for preserving the compositional frequencies was that it enabled the calculation of the minimum folding energy (MFE) without biasing the stabilizing and destabilizing energy from stacked base pairs or loops, respectively (Clote, et al., 2005; Freyhult, et al., 2005; Workman and Krogh, 1999). We used the shuffling strategy implemented in (Clote, et al., 2005), based on the Altschul and Erickson algorithm (Altschul and Erickson, 1985). We use the term “di-shuffle” to represent the shuffling procedure that preserves the mono- and di-nucleotide frequencies of the input sequence. For each known ncRNA sequence in “*Positive936*,” we generated 1,000 di-shuffled sequences, to which we refer as “*Dishuffle936*.”

2.2 Features used

Secondary structures play a key role in the functions of ncRNAs and are more highly conserved than the primary sequences. Accordingly, we investigated a number of secondary structure-based features in terms of their power to differentiate between ncRNAs and their di-shuffled sequences, including novel features such as structural and ensemble statistics, plus a few previously used features such as folding statistics.

Folding statistics: We examined the MFE (Carter, et al., 2001; Wang, et al., 2006; Washietl, et al., 2005) distributions for real ncRNAs and their di-shuffled sequences. Although useful, the current thermodynamic model used in RNA secondary structure prediction is accurate to only within 5-10% of the actual MFE, making the accuracy of the current MFE-based structure predictions around 50-70% (Eddy, 2004). Therefore we used other features in conjunction with MFE to assess the reliability of the secondary structure prediction. One of these features was the Shannon base-pairing entropy measure (Freyhult, et al., 2005; Huynen, et al., 1997). Given an RNA sequence, the Shannon entropy can be computed from the ensemble of predicted secondary structures, as shown in Eqs. 1-2, where $P_{i,j}$ is the probability of base-pairing between nucleotides at sequence positions i and j , and n is the length of the RNA sequence. Note that the higher the entropy, the lower the structural prediction reliability.

$$\text{Shannon base pairing entropy} = \frac{1}{n} \sum_{i=1}^n S_i \quad (1)$$

$$S_i = - \sum_j P_{i,j} \log(P_{i,j}) \quad (2)$$

Fig. S1 (Supplementary Materials) shows the folding statistics (MFE and Shannon entropy) for each ncRNA in *Positive936* compared to *Dishuffle936*. In agreement with (Clote, et al., 2005; Freyhult, et al., 2005), the ncRNAs in our data set were observed to have lower MFE

and Shannon entropy than their di-shuffled sequences.

Ensemble statistics: Besides the Shannon base-pairing entropy, we investigated three other ensemble-based features to assess the global folding reliability among all structures in the Boltzmann ensemble. These features included (1) the free energy of the thermodynamic ensemble, (2) the ensemble diversity statistic computed by RNAfold, and (3) the frequency of the MFE structure. These features measured the average free energy, base-pair distance, and uniqueness of the MFE structure (Gruber, et al., 2008). The free energy of the ensemble for ncRNAs tends to be lower and hence more stable, while the ensemble of ncRNA structures tends to be less diverse, indicating that the ncRNA structures were more unique compared to their di-shuffled decoys, as shown in Fig. S2.

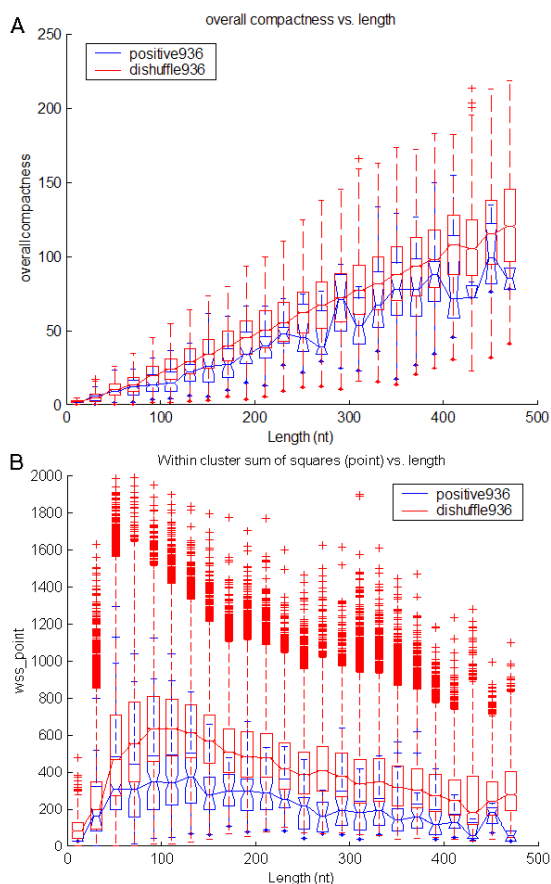


Fig. 1. Ensemble statistics. Boxplots for the (A) overall compactness and (B) within cluster sum of squares vs. sequence lengths for ncRNAs (*Positive936*) and their decoys (*Dishuffle936*). The outliers indicated by the tick marks are values more than two times the inter-quartile range. In general, ncRNAs tended to have fewer clusters that were denser (lower compactness measure) than their decoys, and their within-cluster sum of squares were generally smaller than that of their decoys.

Since the prediction accuracy of secondary structures can improve substantially with the inclusion of suboptimal structures near the MFE (Jaeger, et al., 1989), we applied an RNA secondary structure clustering algorithm, RNACluster (Liu, et al., 2008), to cluster 1,000 predicted structures sampled from all possible secondary structures according to the Boltzmann equilibrium probability distribution (Ding and Lawrence, 2003). Using the base-pairing distance between pre-

dicted secondary structures (Liu, et al., 2008), we calculated various statistics to assess the cluster quality of the sampled structures. One statistic measured the compactness of each cluster (or cluster density) as defined in (Liu, et al., 2008) and shown in Eq. 3, where d_{ij} is the base-pair distance and m is the number of structures within a cluster.

$$\text{compactness} = \frac{\sum_i \sum_j d_{ij}}{m(m-1)} \quad (3)$$

Unlike the clustering analysis of the predicted secondary structures done by the authors of Sfold (Chan and Ding, 2008; Ding, et al., 2005; Ding, et al., 2006), our approach used a rigorous and unique clustering method employed in RNACluster (Liu, et al., 2008). RNACluster identifies dense clusters in the space of all predicted structures by representing the structures as a minimum spanning tree (MST) and by identifying subtrees of the MST that form statistically significant clusters. We calculated five statistics, based on (Chan and Ding, 2008), for discriminating structural RNAs from their decoys using RNACluster: (1) the number of high-frequency base-pairs in the ensemble, (2) the average number of high-frequency base-pairs per cluster, (3) the average base-pair distance between the MFE structure and the ensemble, (4) the between-cluster sum of squares (BSS), and (5) the within-cluster sum of squares (WSS). The BSS statistic measures the base-pair distance between the cluster centroid and the ensemble centroid, while the WSS statistic measures the base-pair distance between the cluster centroid with all structures within that cluster (Chan and Ding, 2008). The centroid definitions may be found in the Supplementary Materials.

We also calculated the BSS and WSS statistics based on a non-optimal ‘centroid’ structure, which we denoted as BSS_point and WSS_point, respectively. The BSS_point measures the between-cluster sum of squares distance between a cluster centroid and the ensemble centroid where the centroid is an existing structure unlike the optimal centroid used in {Chan, 2008 #867}. The WSS_point measures the within-cluster sum of squares distance between the cluster centroid (an actual structure) to all structures within that cluster. In addition, we incorporated the following novel statistics related to the compactness of a cluster: (i) the average compactness, (ii) the maximum compactness, (iii) the minimum compactness, (iv) the compactness of the largest cluster, and (v) the overall compactness to assess the cluster quality generated by RNACluster. Note that the average compactness is the mean of the compactness statistics over all the clusters, while the overall compactness is taken over the entire collection of structures, i.e., the sum of all the distances normalized by the number of structures in the entire collection of structures. The average compactness gives a more localized view of the density of the clusters while the overall compactness gives a more global view of the density of all the structures. Finally, we examined the number of clusters as found by RNACluster.

The statistics calculated by RNACluster were found to be highly discriminatory for separating ncRNAs from their di-shuffled versions, as shown by the P-values in Table S1 (Supplementary Materials). Using the RNACluster method, the structures of known ncRNAs tend to form fewer clusters and be more densely clustered than their di-shuffled versions, as shown in Fig. 1A. Additional compactness-related boxplots are shown in Fig. S3. The statistics from the largest cluster, as shown in Fig. S4, also reflect the same trend for lower compactness statistics in the positive set compared to the di-shuffled set. Our calculation of the relevant statistics from (Chan and Ding, 2008), utilizing RNACluster, agrees with the authors’ results, as shown in Figs. S5-S7 (Supplementary Materials). We showed that our calculation of the WSS_point statistic using RNACluster was more discriminative than the WSS statistic from Sfold in Fig. 1B and S6B, respectively. These results are also reflected in the P-value in Table S1.

Structural statistics: We also considered another set of novel structural features derived from the predicted RNA secondary structures that are useful for the identification of ncRNAs. We examined various properties of known RNA secondary structural elements, i.e., stems and loops

for their possible discerning power between actual ncRNAs and their di-shuffled sequences. For each stem, loop, internal-loop, and bulge structural element, as shown in Fig. S8, we computed the 18 statistics defined in Table S2. To the best of our knowledge, these features have not been applied in the *de novo* identification of ncRNAs.

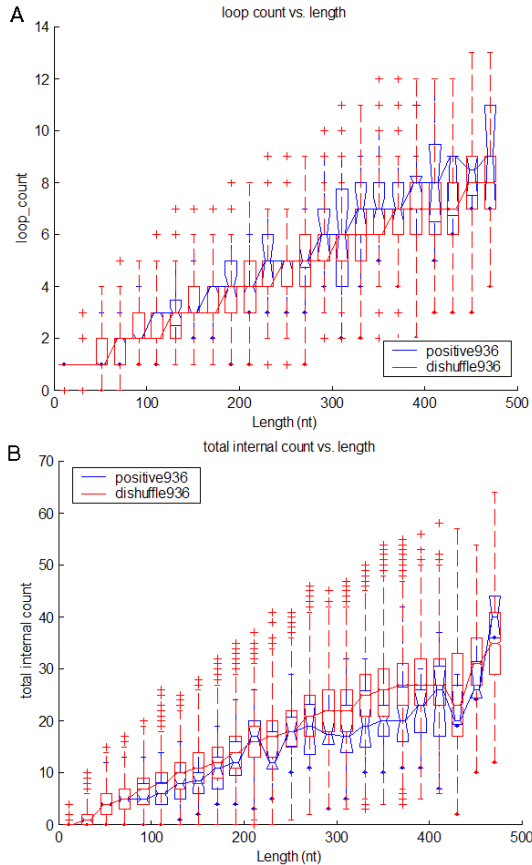


Fig. 2. Structural statistics. Boxplots for the (A) hairpin-loop count and (B) total internal-structure count (internal-loop and bulges) vs. lengths for ncRNAs (*Positive936*) and their decoys (*Dishuffle936*). The outliers indicated by the tick marks are values more than two times the inter-quartile range. In general, ncRNAs tended to have more loop regions and fewer internal-loops on average than their decoys.

From the structural statistics shown in Fig. S9, real ncRNAs tend to have fewer stem branches, but the stems tend to be longer on average. This longer stem preference contributes to more stability in the RNA secondary structure. Real ncRNAs in our dataset also tend to have more loops, as shown in Fig. 2A. The presence of more loops may also be related to the functional role of the ncRNAs. When multiloops are present, there tend to be more loops in real ncRNAs than in their di-shuffled version, as shown in Fig. S10. Not all single-stranded regions were more dominant in real ncRNAs. As seen in Fig. 2B, the total internal-loops consisting of internal loops and bulge regions were actually less in ncRNAs than in their di-shuffled sequences. This tendency for ncRNAs to have fewer of such structural elements may have some functional interpretation that can be applied to ncRNA gene finding. Additional boxplots for loop-related structures are shown in Figs. S11-S12 (Supplementary Materials).

Significant features: For all the features examined above, we used hypothesis testing to identify those features that can potentially distin-

guish known ncRNAs from their di-shuffled sequences. We performed a paired *t*-test, comparing the mean of the features from the *Positive936* data set with the mean from the *Dishuffle936* data set, and computed the P-value estimating the probability that these samples have the same means, as summarized in Table S1. Since the *t*-test assumes distributions of equal variances, we also computed the significance according to the Wilcoxon signed rank because the rank sum test is not based on this assumption; the rank sum test gave similar results. We manually selected a set of 25 features with significant P-values below 0.05, which we refer as the *f25* feature set. This set included two folding statistics, two ensemble statistics, 14 RNAcluster statistics, and seven structural statistics, as shown in Table S1. All features were length normalized (when applicable) before using them for genome-wide prediction. We have also calculated the mean and the variance area under the receiver operating curve (AUROC) for each of the *f25* features in Table 1. The AUROC is a qualitative measure of the performance not dependent on a specific threshold. Generally, the underlying predictor has higher AUROC for higher sensitivity and specificity. Over ten of our features have consistent AUROC values above 0.6. Of additional interest is that some ensemble statistics-based features are found to have higher AUROC values than the commonly used single structure-based MFE measures.

Table 1. The mean and variance for each feature’s AUROC value. The normalized feature values from “Positive936” were compared to 1,000 runs of its “Dishuffle936” to assess each feature’s ability to discriminate between ncRNAs and the corresponding di-shuffled set. The performance below is organism-independent that allows for an unbiased comparison among the features. Over ten features have an average AUROC value above 0.6 that is highly stable across 1,000 runs, each of which uses a different negative set.

Features	mean(AUROC)	var(AUROC)
rnacluster_wss_point	0.7316	5.09E-05
rnacluster_maxcompactness	0.6437	7.14E-05
entropy_entropy	0.6329	5.54E-05
structuralstatistics_stem_ave	0.6325	4.51E-05
diversity_ensemble_diversity	0.6263	8.10E-05
rnacluster_overallcompactness	0.6249	8.07E-05
rnacluster_avecompactness	0.6059	3.18E-05
rnacluster_num_hifreq_bp_ensemble	0.6041	6.27E-05
rnacluster_bss_point	0.6039	7.73E-05
rnacluster_ave_bpdist_mfe_ensemble	0.6011	7.29E-05
rnacluster_compactnesslargest	0.5988	8.54E-05
structuralstatistics_stem_count	0.5960	6.55E-05
rnacluster_ave_num_hifreq_bp_percluster	0.5901	2.00E-05
structuralstatistics_mfe	0.5900	7.04E-06
diversity_free_energy_thermo_ensemble	0.5856	5.94E-06
structuralstatistics_total_internal_count	0.5848	7.69E-05
rnacluster_bss	0.5747	7.59E-05
rnacluster_nclusters	0.5630	3.99E-05
rnacluster_wss	0.5601	6.19E-05
structuralstatistics_total_internal_nt	0.5551	7.77E-05
structuralstatistics_loop_ave	0.5402	8.60E-05
rnacluster_nlargest	0.5292	7.93E-05
rnacluster_mincompactness	0.5237	7.99E-06
structuralstatistics_multiloop_ave	0.5169	5.11E-05
structuralstatistics_loop_count	0.5133	5.96E-05

2.3 Application to genome-wide prediction

In order to construct an unbiased positive set for genome-wide prediction, we included in it all 93 known ncRNAs in *E. coli* from the *Positive1540* data set. Using these ncRNAs as queries, we ran an *all-*

versus-all BLASTN search against the *Positive936* data set and removed all the *Positive936* hits with E-values below 10^{-5} . We reduced the original *Positive936* data set to 800 unique ncRNAs after removing sequences homologous to the 93 known ncRNAs. We then used this data set without known ncRNAs in *E. coli* for training and refer to it as *Positive800_ecoli*.

For the negative set, we di-shuffled 800 randomly selected sequence segments in *E. coli* with the same length distribution as *Positive800_ecoli* to ensure no ncRNA-related secondary structures were present. Other negative training sets were examined but the results were not as significant as the final negative set used. Details of the other negative sets tested can be found in the Supplementary Materials. We computed all the f_{25} significant features and an additional 20 sequence-based statistics, namely, four mono- and 16 di-mer frequencies because they were useful in distinguishing between real ncRNAs and decoys by previous algorithms (Carter, et al., 2001; Klein, et al., 2002; Liu, et al., 2006; Schattner, 2002; Wang, et al., 2006).

Meta-learner classifier to combine information from different window sizes: We applied the genome-wide prediction classifier approach shown in Fig. 3 as follows. For each sample in the training data set, we calculate all 45 features (f_{25} significant features + 20 sequence-based features) within a sliding window of length w which slides from left to the right with step size = $w/2$. The features can undergo a feature ranking selection method before being used to train a window length-specific neural network classifier. The AUROC values of our method using different feature sizes are compared in Table S6.

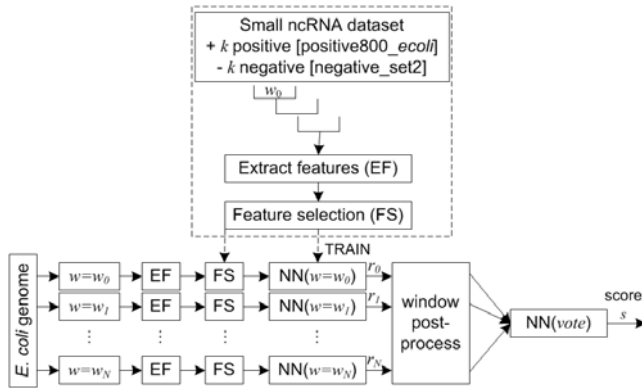


Fig. 3. A schematic of the classifier architecture used for genome-wide prediction. The results of each NN-based classifier were then post-processed and combined into a final NN-based classifier to make the final prediction. The output of the length-specific NN-based classifiers and voting classifier were labeled by score r_i for $0 \leq i \leq N$ and score s , respectively.

Neural networks (NN) are a class of machine learning algorithms, widely used for solving classification problems based on multiple sources of information without assuming the underlying relationships among the individual information sources. This technique is robust for noisy data and has been widely used for many biological data analysis problems (Carter, et al., 2001; Tran, et al., 2007). We have trained an NN-based classifier using MATLAB[®]'s NN toolbox using 45 features derived from our data set. The network parameters were optimized using the Levenberg-Marquardt algorithm to obtain the desired binary (1/0) classification label depending on whether each sample contains an ncRNA or not. Our classifier has a single layer, one-neuron architecture using a logsig activation function. Other NN architectures with more neurons in the current one-layer and two- and three- layer networks were also examined, but the performance improvements were

negligible (data not shown). Our neural network classifier is able to account for the discerning power of each feature and its redundancy in the context of the other features during its training to select an optimal combination of features. We found that using a smaller subset of features (~10-15), we can train a classifier with only slightly lower prediction accuracy (details omitted). We have also used support vector machines to train our classifier but found that the results were not as good (data not shown).

The results from different window length-specific classifiers are combined through a meta-learner neural network classifier to predict the final score. We omit further details about dealing with overlapping windows of different sizes. For testing, we repeated the same procedure using overlapping sliding windows on the entire genome of *E. coli*. By training multiple window length-specific classifiers, each classifier was tuned to distinguish the positive (ncRNAs) from the negative training data for genes of different lengths.

The main computational cost of our approach is in computing the feature set. It takes less than one minute per window to calculate all the features used in the classifier on a 2.2 GHz, 2 GB RAM AMD Opteron dual-processor single-core computer. In order to scan the whole *E. coli* genome using window size $w=120$ requires approximately 54 days on a single processor. Distributed computing is required to make the computation practically feasible.

Filter with positional information to compare with other prediction programs: To reduce the false positive rate in our prediction, we have analyzed the position of known ncRNAs in *E. coli* by classifying all ncRNAs into four classes based on their locations: (1) intergenic, (2) cds_samstrand, (3) antisense, and (4) other cases. The cases of antisense and cds_samstrand were further subcategorized into those ncRNAs that fully or partially overlapped a protein-coding region. We focused on the partially overlapping subcategory because (1) in both *Positive800_ecoli* and our *E. coli* data set, the partially overlapping case was approximately twice as common as the fully overlapping case and (2) experimental validation of fully overlapping cases is difficult (Huttenhofer and Vogel, 2006). For the partially overlapping cases, we computed the log likelihood score using Eq. 4, where $nt_{overlap}$ is the number of overlapped nucleotides between the ncRNA and the protein-coding region. The log likelihood for the antisense and cds_samstrand cases with partial overlap is shown for the *Positive800_ecoli* dataset in Fig. S13. We noted that for the vast majority cases, ncRNA genes partially overlapped protein-coding regions by no more than ~50 nt, which is good for discriminating between the positive and negative sets.

$$LL(nt_{overlap}(ncRNA, CDS)) = \ln \frac{P(nt_{overlap}(ncRNA, CDS)|TP)}{P(nt_{overlap}(ncRNA, CDS)|TN)} \quad (4)$$

2.4 Experimental validation

To identify a manageable list of candidates for experimental validation, we employed data from positional, conservation, promoter, terminator, and a high-density tiling array (Argaman, et al., 2001; Chen, et al., 2002). Conservation denotes candidates with BLASTN hit sequences with E-value $< 10^{-5}$. Promoter and transcription factor binding site information from RegulonDB was used to compile promoter regions within 300 nucleotides upstream of the predicted ncRNA. TransTermHP (Kingsford, et al., 2007) was used to predict rho-independent transcription terminators downstream of our predicted ncRNAs. A tiling array permits an unbiased analysis of complete genomic transcription, including ncRNAs. The whole genome-tiling array data set was derived by comparing an RNase E deletion strain of *E. coli* with a wild type control (Stead *et al.*, manuscript in preparation). This strain was chosen because RNase E has been shown to play an important role in general RNA metabolism in *E. coli* (Bernstein, et al., 2004; Ow and Kushner, 2002). The authors identified 402 possible ncRNA candidates

based on increased steady-state RNA levels in the RNase E deletion strain compared to a wild type control (Stead *et al.*, manuscript in preparation). Overall, we filtered our program's predictions based on the following conditions: (1) the potential ncRNA was conserved; (2) it contained either a predicted promoter or terminator; (3) its overlap with a protein-coding region (if applicable) was < 50 nt; and, (4) it overlapped candidates derived from the tiling array.

Bacterial strains, isolation of total RNA and Northern analysis: The *E. coli* strains used in this study were MG1693 (*thyA715 rph-1*), which was provided by the *E. coli* Genetic Stock Center (Yale University) and an isogenic derivative, SK3564 (*rneA1018::bla thyA715 rph-1 recA56 srlD::Tn10/pDHK30(rng-219 Sm^r/Sp^r)/pWSK129 (Km^r)* which has been described previously (Mohanty and Kushner, 2008). Both strains were grown in Luria broth supplemented with thymine (50 μ g/ml) at 37°C. For MG1693, cells were harvested at 3.5, 6, 8, and 10 hours post-inoculation, corresponding to mid-log, early stationary, mid stationary and late stationary phase growth. For SK3564 the cells were grown in the same manner, but in order to account for its slower growth rate, were harvested at 11.5, 17.5, 20 and 23 hours post-inoculation. Harvested cells were mixed with an equal volume of crushed frozen TM buffer (10 mM Tris [pH 7.2]/5 mM MgCl₂) containing 20 mM Na₃N and 0.4 mg/ml chloramphenicol (O'Hara, et al., 1995). The cells were then centrifuged at 5,000 rpm for 10 min at 4°C. The cell pellets were subsequently resuspended in Trizol[®] (Invitrogen) and total RNA was extracted according to the manufacturer's instructions.

The RNA samples were treated with DNase I using a DNA-free kit[™] (Ambion), ethanol precipitated, quantitated with a Nanodrop apparatus (NanoDrop Technologies) and visualized on 1.0% agarose gels. For Northern analysis, 30 μ g of total RNA were loaded in each lane and separated on either 6% or 8% polyacrylamide/8.3 M urea gels and subsequently transferred onto Magnacharge nylon membranes (GE Water & Processing technologies) by electroblotting (1 h, 80 V, 4°C). Membranes were prehybridized in ULTRAhyb[®] Ultrasensitive Hybridization Buffer (Ambion) at 68°C and probed with internally labeled, *in vitro* transcribed RNA oligomers (oligonucleotide sequences used to generate the probes are available on request). Hybridization was visualized on a Storm 840 PhosphorImager (GE Healthcare).

3 RESULTS

By utilizing folding, ensemble and structure-based features, we developed an NN-based meta-learner for the *de novo* prediction of ncRNAs on a genome-wide scale. We compared our prediction results in *E. coli* to existing programs relying on homology and other information. We found that our results are as good or in some cases better than these methods.

3.1 ncRNA prediction in prokaryotes

Table 2 summarizes the detailed prediction performance of the meta-learner. Our trained meta-learner achieved an average prediction sensitivity of 68%, specificity of 70%, and an overall accuracy of 70% for predicting windows containing ncRNAs in *E. coli*. By combining prediction results from individual window-specific NN-based classifiers, our meta-learner improved the prediction performance of the best individual window-specific classifier. The optimal AUROC performance was achieved using three window sizes, $w = 100, 120,$ and 160 nt, corresponding to the three peaks of the ncRNA-length distribution in *E. coli*, as shown in Fig. S14. The AUROC curve for *E. coli* is given in Fig. S15. For other organisms, users can select a threshold necessary to obtain a desired sensitivity and specificity trade-off for their application.

Table 2. AUROC values of our predictions for *E. coli* and *S. solfataricus* using its optimal three window sizes for both the direct and reverse complement strands.

Organism	Strand	Sn	Sp	AUROC
<i>E. coli</i>	+	0.7182	0.6638	0.7557
<i>E. coli</i>	-	0.6457	0.7275	0.7628
<i>S. solfataricus</i>	+	0.6235	0.7614	0.7502
<i>S. solfataricus</i>	-	0.5149	0.8224	0.7214

We then obtained a unique list of candidates for the genome by labeling continuous regions with NN scores above the user-chosen threshold. The cutoff for the NN threshold will vary depending on the application and the user's preference in trading off the prediction sensitivity and specificity. For our study, we bias in favor of sensitivity rather than missing potential candidates by selecting a low threshold resulting in 16,571 positive candidates. After filtering with positional information by requiring the prediction to (1) fall into an antisense case and (2) have nucleotide overlap < 50 nt with a protein-coding region, we obtained 601 candidates and recovered 41% of known ncRNAs in *E. coli* with a PPV of 6%. 23 of our 601 predicted candidates overlap known strand-specific ncRNAs, four candidates overlapped annotated tRNAs, and 574 novel predictions. A summary of the prediction sensitivity (Sn) and positive prediction values (PPV) for the different programs is summarized in Table 3.

Table 3. Comparison of prediction accuracies by different programs for *E. coli*. The number of predictions, sensitivity (Sn=TP/(TP+FN)), and positive prediction value (PPV=TP/(TP+FP)) is given for each program (Carter, et al., 2001; Chen, et al., 2002; Rivas, et al., 2001; Saetrom, et al., 2005; Wang, et al., 2006).

Program	# predictions	Sn	PPV
Carter	563	0.3441	0.0568
Chen	227	0.2903	0.1189
Rivas	275	0.4086	0.1382
Saetrom	306	0.1183	0.0359
Wang	420	0.0753	0.0167
Tran	601	0.4086	0.0632

Rivas et al. (Rivas, et al., 2001) had an overall better sensitivity and PPV than ours. However, their program relied on prior knowledge of multiple alignments for identification of conserved regions, which may not be generally available for all genomes. Chen et al. (Chen, et al., 2002) had better PPV but lower sensitivity than our program. Compared to (Carter, et al., 2001), we had over 6% improvement in sensitivity with approximately the same PPV. Our predictions were also significantly better in Sn and PPV compared to (Saetrom, et al., 2005) and (Wang, et al., 2006). The results of our *de novo* prediction using structure and sequence-based features is highly promising given the fact that we do not rely on additional promoter/terminator or sequence alignment information as required by other programs. We also illustrated the robustness of our ncRNA predictor by searching for ncRNAs in the thermophilic archaeon, *S. solfataricus* (NC_002754). Our application to *S. solfataricus* yielded an average prediction sensitivity of 57%, specificity of 79%, and an overall accuracy of 71% for predicting windows containing ncRNAs, as shown in Table 2. Additional discussion can be found in the Supplementary Materials.

3.2 Experimental verification of selected ncRNA candidates in *E. coli*

As an application of our *de novo* prediction for use in wet lab studies, we incorporated additional information available to an experimentalist and filtered by conservation, promoter/terminator, positional, and tiling array data to further narrow down our predicted candidates in *E. coli*. Using this filtering approach, we identified 31 candidates as summarized in the Fig. S16 for further validation. Out of the 31 candidates, 17 overlapped with known ncRNA genes or annotated tRNA/rRNA genes in *E. coli*. From the 14 remaining novel predictions, eight were excluded because they overlapped with predicted ncRNA genes derived from other programs (Carter, et al., 2001; Chen, et al., 2002; Rivas, et al., 2001; Saetrom, et al., 2005; Tjaden, et al., 2006; Wang, et al., 2006). The remaining six candidates (#5, 6, 8, 9, 11 and 12), as shown in Table S7, did not overlap with predictions by the other prediction programs, and had higher steady-state levels in the RNase E mutant. Based on our Northern analysis, three of the candidates (5, 6, and 8) were not observed in either the RNase E mutant or the wild type control (data not shown). Since the tiling array has a higher sensitivity than the Northern analysis, we suspect that these potential ncRNAs are transcribed at such low levels that they could not be detected even in the RNase E deletion mutant.

Candidate 9 maps to a region downstream of a predicted strong rho-independent transcription terminator associated with the *ydgA* gene. It also overlaps a repetitive extragenic palindrome called RIP126 (Rudd, 1999). Using an RNA probe of 130 nt, a large species of 480 nt was observed in mid-log phase cells in a wild type strain (data not shown). In addition, significant amounts of smaller species of 140, 170, and 215 nt appeared as the cells entered stationary phase (data not shown). However, because there is considerable nucleotide sequence conservation among the various RIP elements, we designed a second RNA probe (a 30-mer) that was specific for RIP126. With this probe, we observed only the 480 nt species, which was most abundant in both mid-log and early stationary phase cells (Fig. 4A). While we cannot rule out at this time that this species is a stable decay intermediate of the upstream *ydgA* mRNA, based on the predicted strength of the *ydgA* rho-independent transcription terminator, we hypothesize that candidate 9 is indeed a ncRNA that contains a significant region of antisense sequence to the 3' terminus of the adjacent *uidC* mRNA, which is transcribed in the opposite direction.

Candidate 12 is located in the 5' untranslated region (UTR) of the *crp* gene, encoding the catabolite repressor protein. Previous experiments have shown the existence of three potential promoters (P1, P2, and P3) for this gene (Ishizuka, et al., 1994). Transcription initiation from P3 would generate a 5' UTR of 167 nt. The RNA probe used was 89 nt in length and would detect RNA species arising from all three promoters. As shown in Fig. 4C, in exponentially growing wild type cells a large number of discrete species were detected, but most of them rapidly disappeared as the cells entered stationary phase (data not shown). Strikingly, in the RNase E deletion mutant the ~700 nt transcript was the predominant species, demonstrating that almost all of the smaller products observed in the wild type control probably arose from RNase E cleavages. An ~150 nt species was still detected in the RNase E mutant and could have arisen from inefficient cleavages by another endoribonuclease such as RNase G. Since the large species detected in both the RNase E mutant and the wild type control was the approximate size of the full-length *crp* mRNA, we speculate that all of the species observed in wild type cells (Fig. 4C) are probably stable mRNA decay products that retain some or all of the 5' UTR.

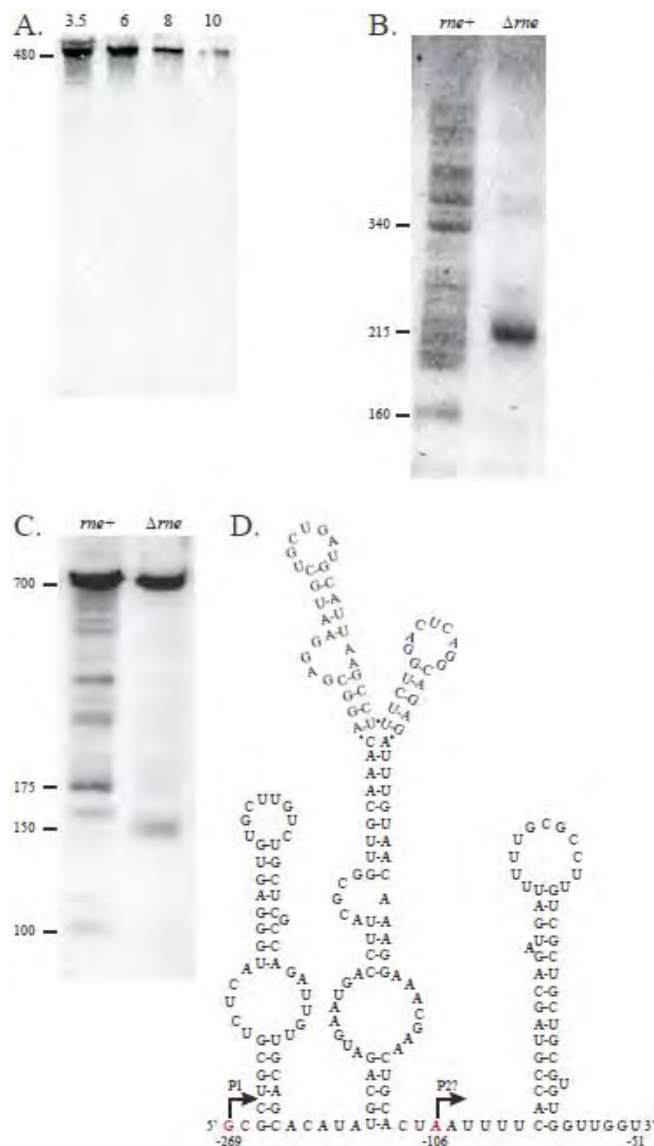


Fig. 4. Analysis of predicted ncRNA candidates 9, 11 and 12. For the Northern blots shown, 30 μ g of total RNA was loaded in each lane and transcript sizes were estimated using a New England Biolabs low range ssRNA ladder. (A) Analysis of candidate 9. RNA isolated from a culture of MG1693 (*rne*⁺) at various times throughout exponential and stationary phase and separated on a 6% PAGE as described in Materials and Methods. (B) Analysis of candidate 11. Total RNA from exponentially growing MG1693 (*rne*⁺) and SK3564 (Δ *rne*) was separated on a 8% PAGE. (C) Analysis of candidate 12. Total RNA from exponentially growing MG1693 (*rne*⁺) and SK3564 (Δ *rne*) were separated on a 6% PAGE. (D) Candidate 11 falls within the 5' UTR of the *mreB* gene. RNAstar secondary structure prediction of a portion of the *mreB* leader (nucleotides -269 to -51). Nucleotides shown in red at positions -269 and -106 correspond to the primer extension products detected by Wachi *et al.* (81). Position -106 was originally identified as a potential transcription start site but may in fact represent an RNase E cleavage site since it occurs in a single-stranded A/U rich region and there is no apparent σ^{70} upstream of this site. Furthermore, we hypothesize that the distal stem-loop that ends of -51 represents a rho-independent transcription terminator that is functional in the Δ *rne* strain.

Candidate 11 falls within the 5' UTR of the *mreB* gene, an essential locus that is involved in establishment of cell shape and cell

division (Shih, et al., 2005). Transcriptional analysis of this gene has identified three potential promoters based on primer extension analysis (Wachi, et al., 2006). Transcription from the most distal promoter would generate a 5' UTR of 267 nt. Using an RNA probe of 145 nt specific for the 5' UTR, we detected numerous species in exponentially growing wild type cells (Fig. 4B). However, in the RNase E deletion mutant, only a single 215 nt species was detected (Fig. 4B). When this 5' UTR fragment was folded using the RNAstar program, a highly structured molecule was predicted (Fig. 4D). We hypothesize that the 215 nt species observed in the RNase E mutant represents a premature termination of transcription of the *mreBCD* operon that arises because of a defect in cell division that is an indirect effect of the reduction in RNase E activity. In wild type cells, where the *mreB* protein is required for normal cell division, transcription proceeds beyond the putative terminator shown in Fig. 4D. Thus our algorithm described here has identified either a riboswitch or a transcription attenuator that is important in the process of bacterial cell division.

4 DISCUSSION

In this study, we identified a number of sequence and structure-based features that can distinguish known ncRNAs from their shuffled versions, which do not rely on *a priori* knowledge of sequence alignments, conservation with closely related organisms, or structural conservation. By utilizing these novel features, we developed a classifier for ncRNA gene prediction. The use of training samples from a large class of ncRNAs from diverse organisms enabled us to find different categories of ncRNAs from various organisms. We have successfully applied our *de novo* predictor to *E. coli* and *S. solfataricus*.

Application of our program has led to a number of novel ncRNA gene predictions. Using Northern blot analysis for *E. coli*, we were able to find expression in three out of six target candidates under our tested conditions. We believe the expressed candidates are stable decay products and one has the potential to be a riboswitch. Further functional experimental studies will be needed in order to fully verify these as real ncRNAs since transcription does not imply function.

The results of our ncRNA prediction in *E. coli* are shown to be highly competitive with or better than the existing prediction programs as we have well demonstrated in this study. Overall our genome-scale prediction results indicate that there may be many more ncRNAs in *E. coli*, particularly in non-intergenic regions, which have been missed by previous studies. Further functional studies on these predicted ncRNA genes are needed to better understand its role and mechanism in regulation.

The promising set of features identified in this study could possibly aid in predicting ncRNAs in eukaryotic genomes. Additional changes to the training set and methodology of the current windowing approach must be made to account for more complex genomic organization in higher-order genomes. Future studies may involve the comparison of other machine learning algorithms and meta-learning approaches.

The *de novo* aspect of our approach makes it easily applicable to newly or partially sequenced genomes since it is not homology-based nor it requires the computation of multiple sequence alignments among related organisms. The ensemble-based features identified in our study perform significantly better than established MFE-based methods. All these capabilities led to the identification of two new regulatory RNAs among other possibly new ncRNA genes.

ACKNOWLEDGEMENTS

We thank the anonymous reviewers for providing valuable suggestions and thank members of the Computational Systems Biology Laboratory for their helpful discussions and Qi Liu for his assistance in using the RNACluster software. We also want to thank Juan Cui for useful discussions and running SVM experiments.

Funding: This work was supported in part by grants from the National Science Foundation (#NSF/DBI-0354771, #NSF/ITR-IIS-0407204, #NSF/DBI-0542119, #NSF/CCF-0621700, #NSF/DBI-0542119004, #NSF/EBI-0542119), the National Institutes of Health (#NIH/1R01GM075331, #NIH/3R01GM075331-01A2S1, #NIH/1R01GM081682-01), the Department of Energy BioEnergy Science Center (#DOE/4000063512) and a Distinguished Scholar grant from the Georgia Cancer Coalition to Y. Xu. The BioEnergy Science Center is a U.S. Department of Energy BioEnergy Research Center supported by the Office of Biological and Environmental Research in the DOE Office of Science. Additional support was provided by the National Institutes of Health (GM057220 and GM081554) to S.R.K.

REFERENCES

- Altshul, S.F. and Erickson, B.W. (1985) Significance of nucleotide sequence alignments: a method for random sequence permutation that preserves dinucleotide and codon usage, *Molecular biology and evolution*, **2**, 526-538.
- Argaman, L., et al. (2001) Novel small RNA-encoding genes in the intergenic regions of *Escherichia coli*, *Curr Biol*, **11**, 941-950.
- Bernstein, J.A., et al. (2004) Global analysis of *Escherichia coli* RNA degradosome function using DNA microarrays, *Proc Natl Acad Sci U S A*, **101**, 2758-2763.
- Carter, R.J., et al. (2001) A computational approach to identify genes for functional RNAs in genomic sequences, *Nucleic Acids Res*, **29**, 3928-3938.
- Chan, C.Y. and Ding, Y. (2008) Boltzmann ensemble features of RNA secondary structures: a comparative analysis of biological RNA sequences and random shuffles, *J Math Biol*, **56**, 93-105.
- Chen, S., et al. (2002) A bioinformatics based approach to discover small RNA genes in the *Escherichia coli* genome, *Biosystems*, **65**, 157-177.
- Clote, P., et al. (2005) Structural RNA has lower folding energy than random RNA of the same dinucleotide frequency, *Rna*, **11**, 578-591.
- Coventry, A., et al. (2004) MSARI: multiple sequence alignments for statistical detection of RNA secondary structure, *Proc Natl Acad Sci U S A*, **101**, 12102-12107.
- di Bernardo, D., et al. (2003) ddbRNA: detection of conserved secondary structures in multiple alignments, *Bioinformatics*, **19**, 1606-1611.
- Ding, Y., et al. (2005) RNA secondary structure prediction by centroids in a Boltzmann weighted ensemble, *Rna*, **11**, 1157-1166.
- Ding, Y., et al. (2006) Clustering of RNA secondary structures with application to messenger RNAs, *J Mol Biol*, **359**, 554-571.
- Ding, Y. and Lawrence, C.E. (2003) A statistical sampling algorithm for RNA secondary structure prediction, *Nucleic Acids Res*, **31**, 7280-7301.
- Eddy, S.R. (2004) How do RNA folding algorithms work?, *Nat Biotechnol*, **22**, 1457-1458.
- Enright, A.J., et al. (2002) An efficient algorithm for large-scale detection of protein families, *Nucleic Acids Res*, **30**, 1575-1584.
- Freyhult, E., et al. (2005) A comparison of RNA folding measures, *BMC Bioinformatics*, **6**, 241.
- Gaspin, C., et al. (2000) Archaeal homologs of eukaryotic methylation guide small nucleolar RNAs: lessons from the *Pyrococcus* genomes, *J Mol Biol*, **297**, 895-906.
- Gottesman, S. (2005) Micros for microbes: non-coding regulatory RNAs in bacteria, *Trends Genet*, **21**, 399-404.
- Gruber, A.R., et al. (2008) The Vienna RNA Websuite, *Nucleic Acids Res*.
- Huttenhofer, A., et al. (2002) RNomics: identification and function of small, non-messenger RNAs, *Curr Opin Chem Biol*, **6**, 835-843.
- Huttenhofer, A. and Vogel, J. (2006) Experimental approaches to identify non-coding RNAs, *Nucleic Acids Res*, **34**, 635-646.
- Huynen, M., et al. (1997) Assessing the reliability of RNA folding using statistical mechanics, *J Mol Biol*, **267**, 1104-1112.
- Ishizuka, H., et al. (1994) Mechanism of the down-regulation of cAMP receptor protein by glucose in *Escherichia coli*: role of autoregulation of the *crp* gene, *EMBO J*, **13**, 3077-3082.
- Jaeger, J.A., et al. (1989) Improved predictions of secondary structures for RNA, *Proc Natl Acad Sci U S A*, **86**, 7706-7710.
- Kingsford, C.L., et al. (2007) Rapid, accurate, computational discovery of Rho-independent transcription terminators illuminates their relationship to DNA uptake, *Genome Biol*, **8**, R22.

- Klein, R.J., et al. (2002) Noncoding RNA genes identified in AT-rich hyperthermophiles, *Proc Natl Acad Sci U S A*, **99**, 7542-7547.
- Larsson, P., et al. (2008) De novo search for non-coding RNA genes in the AT-rich genome of *Dictyostelium discoideum*: performance of Markov-dependent genome feature scoring, *Genome Res*, **18**, 888-899.
- Liu, C., et al. (2005) NONCODE: an integrated knowledge database of non-coding RNAs, *Nucleic Acids Res*, **33**, D112-115.
- Liu, J., et al. (2006) Distinguishing protein-coding from non-coding RNAs through support vector machines, *PLoS Genet*, **2**, e29.
- Liu, Q., et al. (2008) RNAcluster: An integrated tool for RNA secondary structure comparison and clustering, *J Comput Chem*, **29**, 1517-1526.
- Livny, J., et al. (2005) sRNAPredict: an integrative computational approach to identify sRNAs in bacterial genomes, *Nucleic Acids Res*, **33**, 4096-4105.
- Mohanty, B.K. and Kushner, S.R. (2008) Rho-independent transcription terminators inhibit RNase P processing of the secG leuU and metT tRNA polycistronic transcripts in *Escherichia coli*, *Nucleic Acids Res*, **36**, 364-375.
- O'Hara, E.B., et al. (1995) Polyadenylation helps regulate mRNA decay in *Escherichia coli*, *Proc Natl Acad Sci U S A*, **92**, 1807-1811.
- Ow, M.C. and Kushner, S.R. (2002) Initiation of tRNA maturation by RNase E is essential for cell viability in *E. coli*, *Genes Dev*, **16**, 1102-1115.
- Pedersen, J.S., et al. (2006) Identification and classification of conserved RNA secondary structures in the human genome, *PLoS Comput Biol*, **2**, e33.
- Pichon, C. and Felden, B. (2003) Intergenic sequence inspector: searching and identifying bacterial RNAs, *Bioinformatics*, **19**, 1707-1709.
- Rivas, E. and Eddy, S.R. (2000) Secondary structure alone is generally not statistically significant for the detection of noncoding RNAs, *Bioinformatics*, **16**, 583-605.
- Rivas, E. and Eddy, S.R. (2001) Noncoding RNA gene detection using comparative sequence analysis, *BMC Bioinformatics*, **2**, 8.
- Rivas, E., et al. (2001) Computational identification of noncoding RNAs in *E. coli* by comparative genomics, *Curr Biol*, **11**, 1369-1373.
- Rudd, K.E. (1999) Novel intergenic repeats of *Escherichia coli* K-12, *Res Microbiol*, **150**, 653-664.
- Saetrom, P., et al. (2005) Predicting non-coding RNA genes in *Escherichia coli* with boosted genetic programming, *Nucleic Acids Res*, **33**, 3263-3270.
- Schattner, P. (2002) Searching for RNA genes using base-composition statistics, *Nucleic Acids Res*, **30**, 2076-2082.
- Shih, Y.L., et al. (2005) The MreB and Min cytoskeletal-like systems play independent roles in prokaryotic polar differentiation, *Mol Microbiol*, **58**, 917-928.
- Szymanski, M., et al. (2003) Noncoding RNA transcripts, *J Appl Genet*, **44**, 1-19.
- Tjaden, B., et al. (2006) Target prediction for small, noncoding RNAs in bacteria, *Nucleic Acids Res*, **34**, 2791-2802.
- Tran, T.T., et al. (2007) Operon prediction in *Pyrococcus furiosus*, *Nucleic Acids Res*, **35**, 11-20.
- Wachi, M., et al. (2006) Transcriptional analysis of the *Escherichia coli* mreBCD genes responsible for morphogenesis and chromosome segregation, *Biosci Biotechnol Biochem*, **70**, 2712-2719.
- Wang, C., et al. (2006) PSoL: a positive sample only learning algorithm for finding non-coding RNA genes, *Bioinformatics*, **22**, 2590-2596.
- Washietl, S., et al. (2005) Fast and reliable prediction of noncoding RNAs, *Proc Natl Acad Sci U S A*, **102**, 2454-2459.
- Wassarman, K.M., et al. (2001) Identification of novel small RNAs using comparative genomics and microarrays, *Genes Dev*, **15**, 1637-1651.
- Workman, C. and Krogh, A. (1999) No evidence that mRNAs have lower folding free energies than random sequences with the same dinucleotide distribution, *Nucleic Acids Res*, **27**, 4816-4822.
- Yachie, N., et al. (2006) Prediction of non-coding and antisense RNA genes in *Escherichia coli* with Gapped Markov Model, *Gene*, **372**, 171-181.
- Zhang, Y., et al. (2004) Conservation analysis of small RNA genes in *Escherichia coli*, *Bioinformatics*, **20**, 599-603.